Magnetism in 2D materials for spintronics application

M.Sc Thesis

By

Hiba K.P



DEPARTMENT OF PHYSICS INDIAN INSTITUTE OF TECHNOLOGY INDORE May 2025

CANDIDATE'S DECLARATION

I hereby certify that the work which is being presented in this thesis entitled "Magnetism in 2D materials for spintronics application" in the partial fulfillment of the requirements for the award of the degree of MASTER OF SCIENCE and submitted in the DEPARTMENT OF PHYSICS, Indian Institute Of Technology Indore, is an authentic record of my own work carried out during the time period from June 2024 to May 2025 under the supervision of Dr. Preeti A. Bhobe, Professor, Department of Physics, Indian Institute of Technology Indore.

The matter presented in this thesis has not been submitted by me for the award of any other degrees of this or any other institute.

OXD

| | () Hoa |
|---|---------------------------------|
| | Hiba K.P |
| | |
| | |
| This is to certify that the above statement made by | the candidate is correct to the |
| best of my knowledge. | |
| | Poti |
| | Prof. Preeti A. Bhobe |
| | |
| | |

Hiba K.P, has successfully given her M.Sc. Oral examination held on 14/05/2025.

Supervisor Signature

Prof. Preeti A. Bhobe

Date: 20/05/2025 Date:20/05/2025

DPGC Signatute

ACKNOWLEDGEMENT

First and foremost, I would like to express my sincere gratitude to my project supervisor, Prof. Preeti A. Bhobe, for her continuous guidance and support throughout the course of this work. Her patience and encouragement during the challenging phases of the project kept me motivated, and her approachability fostered a supportive environment for open discussions. I am also deeply thankful for her valuable suggestions during report writing and presentations, which significantly enhanced my academic development.

I extend my sincere thanks to Prof. Somaditya Sen for the powder XRD measurements, and to Prof. Elaine Dias from Goa University for magnetic measurements. I also appreciate the support provided by SIC Indoor for access to various facilities. My gratitude goes to the Department of Physics and IIT Indore for the infrastructure and opportunities that made this work possible.

I am especially thankful to my senior lab mate, Astha Tiwari, for her patient guidance in teaching me the operation and handling of various laboratory instruments and for her continued support throughout the project. I would also like to acknowledge Ramavatar Devanda, Aarti Lakhara, Aman Kumar, Ashish Meena, and other lab members for their consistent help, guidance, and cooperation.

I deeply value the companionship of my friends, whose presence made for a pleasant and stress-free work environment.

Most importantly, I am profoundly grateful to my parents and siblings for their constant encouragement and unwavering belief in me.

ABSTRACT

This project focuses on the synthesis and magnetic characterization of twodimensional (2D) magnetic materials for potential spintronics applications. Fe₃GeTe₂ and VSe₂ were synthesized and studied in detail to understand their magnetic behavior, with particular attention to the effects of stoichiometric deviations and structural defects. Additionally, other 2D materials—ZrSe₂, ZrSe₃, and TiSe₂—synthesized by lab colleagues, were examined to explore their intrinsic and defect-induced magnetic properties. Various characterization techniques, including powder X-ray diffraction (PXRD), energy-dispersive X-ray spectroscopy (EDX), Raman spectroscopy, resistivity, and magnetic measurements, were employed. While the synthesis of Fe₃GeTe₂ was hindered by tellurium loss, VSe₂, although successfully forming the desired phase, exhibited deviations from the ideal stoichiometry. Magnetic measurements across other 2D chalcogenides revealed behaviors ranging from diamagnetism to paramagnetism, depending on factors such as composition and doping. These findings underscore the sensitivity of magnetism in 2D materials to structural and compositional variations and highlight their potential for next-generation magnetic and spintronic devices.

Contents

| 1 | Intr | oductio | n | 1 |
|---|--|---------|---|----|
| 2 | Material synthesis and characterization techniques | | | 9 |
| | 2.1 | Prepar | ation of Fe ₃ GeTe ₂ | 9 |
| | | 2.1.1 | Attempt 1: Chemical Vapor Transport (CVT) Method | 9 |
| | | 2.1.2 | Attempt 2: Polycrystalline Precursor via Solid-State Reaction | 10 |
| | | 2.1.3 | Final Attempt with Tellurium Compensation | 11 |
| | 2.2 | Prepar | ation of VSe ₂ | 11 |
| | | 2.2.1 | Solid-State Method | 11 |
| | | 2.2.2 | Chemical Vapor Transport (CVT) Method | 12 |
| | | 2.2.3 | Annealing for Stoichiometric Correction | 13 |

| | 2.3 | Charac | eterization techniques | 13 |
|---|------|---------------------------------|--|----|
| | | 2.3.1 | X-ray diffraction | 13 |
| | | 2.3.2 | Raman spectroscopy | 15 |
| | | 2.3.3 | Energy-dispersive X-ray analysis | 16 |
| | | 2.3.4 | Resistivity | 17 |
| | | 2.3.5 | Magnetic measurement | 18 |
| • | Dage | des and | Discussion | 22 |
| 3 | Rest | ms and | Discussion | 23 |
| | 3.1 | Fe ₃ Ge ⁷ | Ге ₂ | 23 |
| | | 3.1.1 | Initial CVT Sample | 23 |
| | | 3.1.2 | Polycrystalline Sample | 24 |
| | | 3.1.3 | Single Crystal Sample | 25 |
| | | 3.1.4 | Te Compensation and Characterization | 26 |
| | 3.2 | VSe ₂ . | | 28 |
| | | 3.2.1 | Solid-State Synthesized VSe ₂ | 28 |
| | | 3.2.2 | CVT Synthesized VSe ₂ | 31 |
| | 3.3 | Magne | etic measurements | 34 |
| | | 3.3.1 | ZrSe ₂ | 34 |

| 4 | Conclusion | | 40 |
|---|------------|-------------------|----|
| | 3.3.3 | TiSe ₂ | 37 |
| | 3.3.2 | ZrSe ₃ | 36 |

Chapter 1

Introduction

Magnetism is a physical phenomenon created by the orbital and angular motion of electrons. Depending on the interaction between orbital and angular moments and the response to the external magnetic field, magnetism is classified as paramagnetism, diamagnetism, ferromagnetism, antiferromagnetism, and ferrimagnetism. Magnetic interactions, such as dipolar and exchange interactions, are responsible for the long-range ordering of magnetic moments. The exchange interaction is the one that plays a major role in magnetic ordering for materials with a higher Curie temperature (T_c). Where T_c is the temperature above which the randomizing tendency by thermal fluctuation wins over the ordering property of a material. Exchange interactions can be of different types.

• **Dipolar interaction:** Energy of two magnetic dipoles μ_1 and μ_2 separated

by a distance \vec{r} is given by,

$$E = \frac{\mu_0}{4\pi r^3} \left[\mu_1 \cdot \mu_2 - \frac{3(\mu_1 \cdot \vec{r})(\mu_2 \cdot \vec{r})}{r^2} \right]$$
 (1.1)

By taking $\mu_1 = \mu_2 \approx 1 \mu_b$ and $r \approx 1 A^0$, we can calculate the energy be approximately equals to 10^{-4} eV. Converting this to equivalent temperature gives 1 K. Since most of the materials have a T_c higher than this, we can conclude that dipole interaction is only relevant for materials that get ordered at millikelvin temperature.

• Exchange interaction: Exchange interaction is an electrostatic interaction that arises as charges of the same sign repel each other while coming together. When we consider electrons, the wave function should be antisymmetric. This anti-symmetrization brings about a spin-dependent term in energies even though the Coulomb interaction doesn't care about spins, i.e., the energy of triplet (E_T) is different from the energy of singlet (E_S) . The separation of energy scales of E_T and E_S is of the order we are looking for. We can write the Hamiltonian of a two-electron system as,

$$\mathbf{H} = \frac{1}{4} (E_S + E_T) - (E_S - E_T) \mathbf{S_1} \cdot \mathbf{S_2}$$
 (1.2)

By absorbing the constant term in this equation into other constant energy terms, we can rewrite the Hamiltonian as,

$$\mathbf{H_{spin}} = -2J\mathbf{S_1} \cdot \mathbf{S_2} \tag{1.3}$$

Here, $J = \frac{(E_S - E_T)}{2}$ is called as the exchange constant. Equation (1.3) distin-

guishes between parallel and anti-parallel spins depending on the sign of J. For a many-body system, according to the Heisenberg model, we can write the Hamiltonian as,

$$\mathbf{H} = -2\sum_{i,j} J_{i,j} \mathbf{S_1} \cdot \mathbf{S_2} \tag{1.4}$$

where $J_{i,j}$ is the exchange constant between i^{th} and j^{th} spins. If we neglect the interactions of moments with moments other than the nearest neighbors, the Hamiltonian can be modified as,

$$\mathbf{H} = -2\sum_{\langle i,j\rangle} J_{i,j} \mathbf{S_1} \cdot \mathbf{S_2} \tag{1.5}$$

which is called the nearest neighbor Heisenberg model.

The exchange interaction so far discussed is called direct exchange. In direct exchange, magnetic ions sit next to each other such that their wave functions can overlap. If there is a non-magnetic ion between two magnetic ions, then it's called a super-exchange. Here, the waves of magnetic ions do not overlap, but they interact via non-magnetic ions. There is another type of interaction that arises when there are conduction electrons between magnetic ions, which is called RKKY interaction (or itinerant exchange). In RKKY interaction, the magnetic ion polarises conduction electrons, which pass information to the next magnetic ion. The exchange interaction $J_{RKKY}(r)$ is given as,

$$J_{RKKY}(r) \propto \frac{cos(2k_F r)}{r^3}$$
 (1.6)

Here, r is the distance between magnetic ions, and r_F is the radius of the Fermi surface. Whether the interaction is ferromagnetic or antiferromagnetic

depends on the distance r since J_{RKKY} depends on the cosine of r. This interaction usually occurs between electrons in partially filled f-shells in rare-earth metals[1].

Our focus is on magnetism in two-dimensional (2D) materials. These materials are crystalline structures composed of only a few atomic layers, where strong inplane interactions interactions dominate over the comparatively weak inter-layer stacking interactions. Because the layers are held together by weak van der Waals forces, the material can be exfoliated one layer at a time. This weak inter-layer bonding also leads to the confinement of physical properties within the two-dimensional planes.

Magnetism in 2D materials is of significant interest due to its potential applications in spintronics. Spintronics, unlike conventional electronics, utilizes not only the charge of the electron but also its spin for information processing and transfer. The spin-up and spin-down states of electrons can represent binary data—0 and 1—enabling data storage. Incorporating 2D magnetic materials into spintronic devices offers the advantage of significantly reducing device size without compromising performance. Materials like CrI₃ and Cr₂Te₃ exhibit long-range magnetic order; however, their low magnetic transition temperatures make them unsuitable for practical spintronics applications. Therefore, attention is directed toward Fe₃GeTe₂ and VSe₂, which exhibit transition temperatures nearer to room temperature. This improved thermal stability is attributed to their strong magnetic crystalline anisotropy, which helps suppress thermal fluctuations.

Fe₃GeTe₂ is an itinerant ferromagnet with the c-axis as the easy axis of magnetization. It has a hexagonal structure and belongs to the P6₃/mmc space group.

The results derived from the vibrating sample magnetometer (VSM) are given

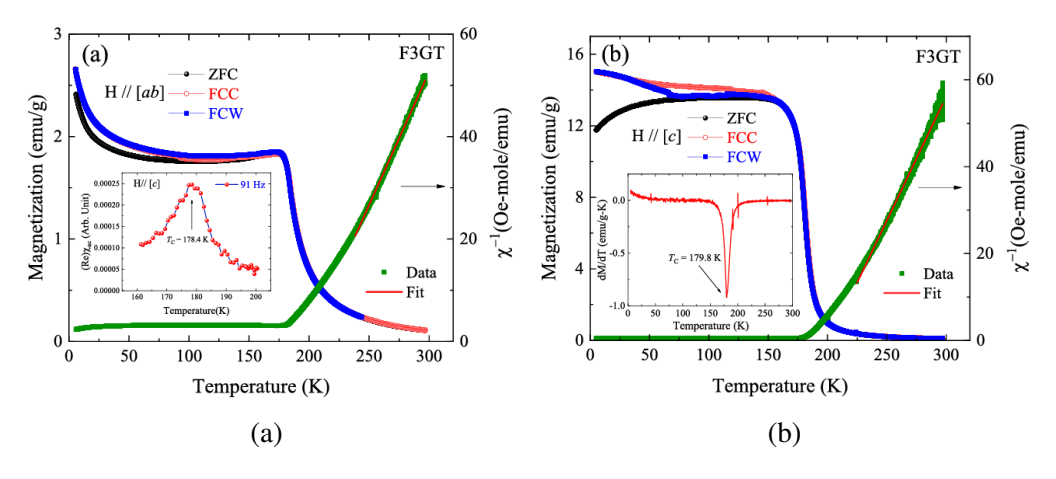


Figure 1.1: magnetic field applied (a) along the ab plane and (b) along c [2].

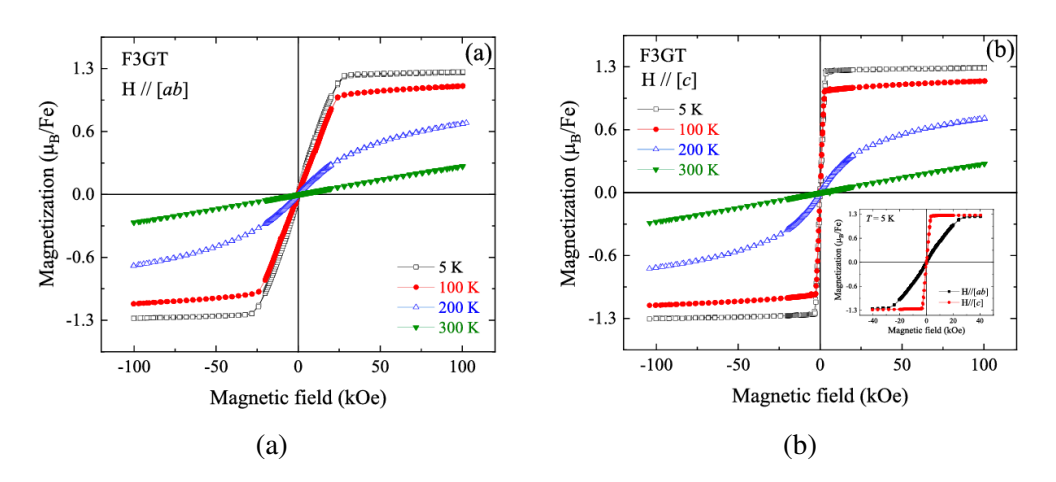


Figure 1.2: Magnetic field dependence of isothermal magnetization curves for field applied along (a)ab plane and (b)crystallographic c direction [2]

in Figure 1.1. Here in zero-field-cooling (ZFC), the sample is cooled from room temperature to 5 K in the absence of an external magnetic field, and then at 5 K, an external field of 1 kOe is applied, and the data were collected while warming the

sample. In field-cooled cooling (FCC), the sample is cooled from room temperature to 5 K in the presence of an external magnetic field of 1 kOe, and the data were collected along with the cooling. Field-cooled-warming (FCW) data are taken as a continuation of FCC, i.e., after cooling in FCC, the sample is again warmed, and the data collected at that time are plotted in FCW. From this data, we can infer that there is a significant magnetocrystalline anisotropy. The magnetic moments $\frac{M_{ab}}{M_c}$ along magnetically ordered states conform to c as the easy axis of magnetization. In Figure 1.2, we can see that hysteresis loss is negligible, indicating that Fe₃ GeTe₂ is a soft ferromagnet. The reduction in saturation magnetization when compared to that of free iron (2.216 μ_B) may hint at the itinerant character of iron 3d electrons in this compound. T_c (140 K- 230 K) of Fe₃GeTe₂ varies according

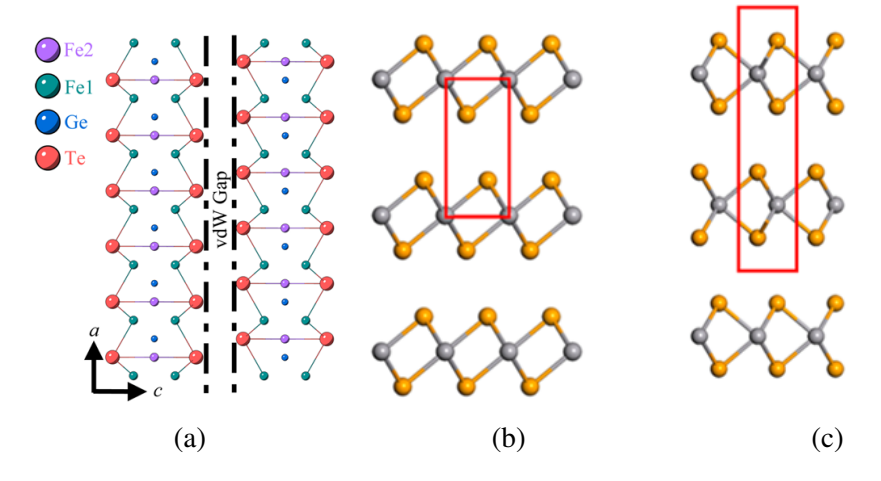


Figure 1.3: (a) Crystal structure of Fe₃GeTe₂.(b) 2H-VSe₂, and (c) 1T-VSe₂. Gray and orange balls represent V and Se atoms, respectively [3].

to the concentration of Fe [2]. The higher the Fe concentration, the larger the T_c . The flux-grown crystals have reduced Fe content compared to crystals grown by the chemical vapour transport (CVT) method, hence, they have low T_c . Usually,

the low concentration of Fe is exhibited as a vacancy in the Fe_{II} site. As the Fe content decreases, there will be a slight decrease in the lattice parameter, a, and a slight increase in c [4]. These changes impact its magnetic interactions. Hence, our objective in this work is to study the effect of such defects on the magnetic properties of Fe₃GeTe₂.

Similarly, defects and structural variations also play a significant role in determining the magnetic behavior of VSe₂. This material exists in multiple phases, with 1T and 2H being the most prominent. These phases differ in structure (Figure 1.3), leading to distinct physical properties. For instance, while the 1T phase exhibits metallic behavior, the 2H phase is semiconducting. This study aims to explore how different phases influence magnetism, along with the role of defects in modifying the magnetic properties.

Chapter 2

Material synthesis and characterization techniques

2.1 Preparation of Fe₃GeTe₂

2.1.1 Attempt 1: Chemical Vapor Transport (CVT) Method

Fe₃GeTe₂ was initially prepared using the chemical vapor transport (CVT) method. High-purity elemental powders of Fe, Ge, and Te were mixed in a molar ratio of 3:1:2. Iodine powder (5 mg/cm³) was added as a vapor transport agent. The mixture was loaded into a 20 cm long evacuated quartz tube, which was then sealed.

The tube was placed in a horizontal two-zone tube furnace with one end set at

750 °C and the other at 700 °C. The setup was maintained under these conditions for one week.

2.1.2 Attempt 2: Polycrystalline Precursor via Solid-State Reaction

Due to challenges in the CVT approach, a revised synthesis strategy was employed with the goal of stabilizing the desired phase in polycrystalline form before attempting single-crystal growth.

Polycrystalline Synthesis

High-purity Fe, Ge, and Te powders were weighed in stoichiometric proportions and thoroughly ground inside a nitrogen-filled glove box. The homogeneous powder mixture was sealed in an evacuated quartz ampule and subjected to solid-state reaction in a muffle furnace.

The furnace was heated to 600 °C at a rate of 60 °C/hour. The temperature was maintained for 5 days, followed by in-furnace cooling to room temperature.

Single Crystal Growth

The resulting polycrystalline sample was finely ground and pelletized. The pellet, along with iodine (5 mg/cm³), was sealed in a quartz tube. Single-crystal growth was attempted using the vapor transport technique in a horizontal two-zone furnace.

The hot zone was set to 700 °C, and the cold zone to 650 °C, with a ramp rate of 1 °C/min. The synthesis was carried out for 10 days, after which the sample was furnace-cooled.

2.1.3 Final Attempt with Tellurium Compensation

Following initial difficulties in forming the desired phase, all previously synthesized Fe₃GeTe₂ samples were combined and ground. An additional 5% excess of Te was added to the stoichiometric mix to compensate for possible evaporation losses observed in earlier attempts.

The final mixture was pelletized and sealed in a quartz ampule. It was then subjected to a solid-state reaction at 600 °C for 5 days, with both heating and cooling rates controlled at 1 °C/hour. This procedure aimed to enhance phase stability and improve stoichiometric integrity.

A subsequent annealing process was carried out under identical conditions.

2.2 Preparation of VSe₂

2.2.1 Solid-State Method

The vanadium required for the preparation was initially in rod form. To process it, the rod was cut into small pieces using a diamond cutter and then pressed into thin pellets. These pellets, along with selenium powder, were placed in a muffle

furnace at 850 °C for three days, with a heating and cooling rate of approximately 5 °C per hour, to facilitate the melting of the vanadium pellets.

Since some of the vanadium did not melt completely, a second round of synthesis was performed. To ensure proper stoichiometry, an additional amount of selenium, with a 3% excess, was added, and the process was repeated, reducing the duration to two days instead of three.

Afterward, the sample was annealed under the same furnace conditions for an additional 3 days.

2.2.2 Chemical Vapor Transport (CVT) Method

High-purity vanadium and selenium powders were mixed in a 1:2 molar ratio and pressed into a pellet. The pellet was combined with 63 mg of iodine powder and loaded into a 25 cm long evacuated quartz tube. The tube was sealed and placed in a horizontal two-zone tube furnace.

The temperature profile was as follows:

- Heated to 450 °C (hot zone) / 350 °C (cold zone) at 5 °C/min, held for 1 hour.
- Increased to $550\,^{\circ}\text{C}$ / $450\,^{\circ}\text{C}$, held for 1 hour.
- Continued incrementally to 850 °C / 750 °C, with each step held for 1 hour.
- Finally, held at 850 °C / 750 °C for 3 days before furnace cooling.

2.2.3 Annealing for Stoichiometric Correction

To improve the stoichiometry, the single-crystalline and polycrystalline VSe₂ samples obtained from this CVT process were combined and subjected to the same synthesis conditions once again. However, during this attempt, no single crystals were formed.

2.3 Characterization techniques

Several characterization techniques—including powder X-ray diffraction (P-XRD), Energy-dispersive X-ray (EDX), Raman spectroscopy, resistivity measurements, and magnetic measurements—were employed to verify the material's successful formation and its physical properties.

2.3.1 X-ray diffraction

X-ray diffraction (XRD) is a non-destructive technique used to determine various properties of crystalline materials, such as crystal structure, phase composition, lattice parameters, and crystallite size. The principle behind XRD is based on the diffraction phenomenon, where atoms arranged periodically in a crystalline structure act as scattering centers for X-rays. The diffraction condition is governed by Bragg's law, which is expressed as:

$$n\lambda = 2d\sin\theta\tag{2.1}$$

In this equation:

- n is the order of diffraction
- λ is the wavelength of X-ray
- d is the distance between atomic planes
- θ is the angle of incidence with respect to the diffraction plane

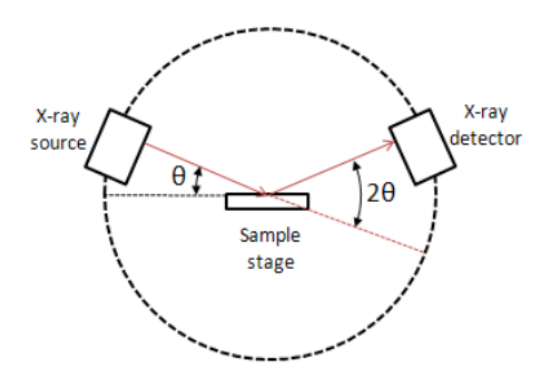


Figure 2.1: Schematic of XRD setup in Bragg-Brentano geometry

In powder X-ray diffraction (P-XRD), the X-ray wavelength (λ) is constant while the angle (θ) is varied. For laboratory-based measurements, the Bragg-Brentano geometry (Figure 2.1) is commonly employed, where the sample remains stationary while both the incident X-ray beam and the detector move symmetrically. The resulting data is typically presented as a plot of intensity versus 2θ . From this plot, the d-spacing can be determined using Bragg's law (Equation (2.1)). By comparing the calculated d-spacing values with known references from the International Center for Diffraction Data (ICDD), the phases present in the sample can be identified, among other analyses.

2.3.2 Raman spectroscopy

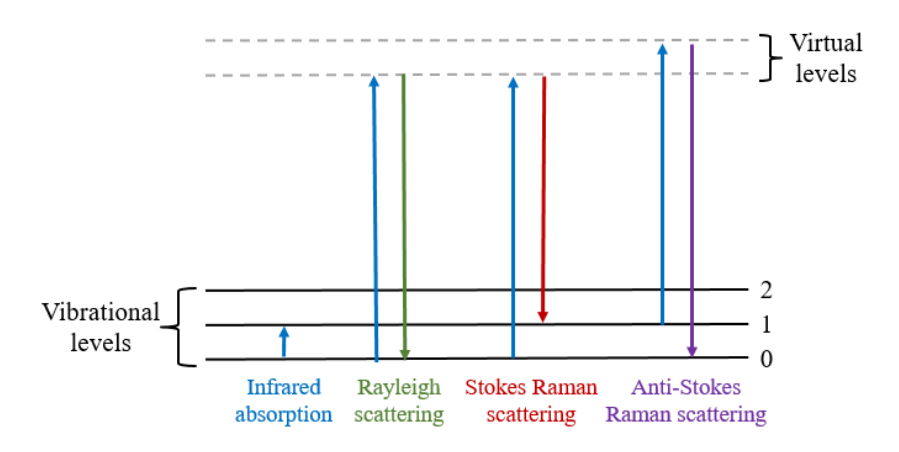


Figure 2.2: Energy level diagram showing Rayleigh and Raman scattering.

Raman spectroscopy is a non-destructive analytical technique primarily used to detect changes in molecular vibrations and to provide insights into concentration, chemical structure, and molecular symmetry. It is based on Raman scattering, which refers to the inelastic scattering of light. For a molecular vibration or rotation to be Raman active, it must induce a change in the molecule's polarizability. In a typical Raman experiment, the energy difference between the incident light and the scattered photons is measured. Depending on whether the scattered photon has lower or higher energy than the incident photon, the process is classified as Stokes or anti-Stokes Raman scattering, respectively (Figure 2.2). The results are commonly presented as a plot of Raman intensity versus Raman shift, where the Raman shift (in units of wavenumbers) represents the relative energy difference between the incident and scattered light.

2.3.3 Energy-dispersive X-ray analysis

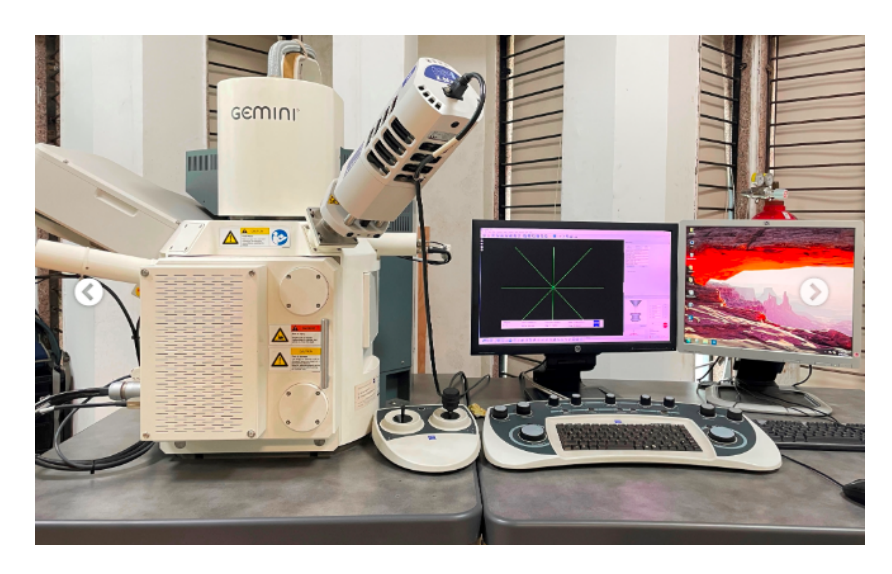


Figure 2.3: FE-SEM with EDX setup.

Energy Dispersive X-ray Spectroscopy (EDS/EDX) is a technique used to determine the elemental composition of a material. It is commonly coupled with scanning electron microscopy (SEM) or scanning transmission electron microscopy (STEM) to obtain both structural images and compositional data simultaneously (Figure 2.3). In this method, a high-energy electron beam is directed onto the sample, causing the ejection of inner-shell (core) electrons and creating vacancies. These vacancies are then filled by electrons from higher energy levels, releasing characteristic X-rays specific to each element in the process. By analyzing the energies and intensities of these X-rays, both the identity and relative concentration of the elements present in the sample can be determined.

2.3.4 Resistivity



Figure 2.4: Resistivity setup.

Resistance measurements were performed using a CCR (Closed-Cycle Refrigerator)-based laboratory system, as shown in Figure 2.4. Depending on the sample, either the two-probe or four-probe method was employed. In the two-probe technique, current is applied through one probe while the voltage is measured across the second. This method is suitable for high-resistance materials, such as insulators, where the influence of contact resistance is negligible. However, for low-resistance materials like metals and semiconductors, contact resistance can significantly affect the measurements. Therefore, the four-probe method is preferred for such samples. In the four-probe configuration, the outer two probes supply the current while the inner two measure the voltage. Due to the high internal impedance of the voltmeter, the current through the voltage probes is minimal, effectively eliminating the impact of contact resistance.

Once the resistance R is obtained, the resistivity ρ of the sample can be calculated using the relation:

$$\rho = \frac{RA}{l} \tag{2.2}$$

Where:

- A is the cross-sectional area of the rectangular sample,
- *l* is the distance between the voltage probes.

2.3.5 Magnetic measurement

There are different methods for measuring the magnetic properties of a material. Mainly, a superconducting quantum interference device (SQUID) and a vibrating sample magnetometer (VSM) are used.

SQUID

Superconducting quantum interference device is a highly sensitive (about 10⁵ T) magnetic field measurement device. SQUID works using superconductivity, the Josephson effect, and magnetic flux quantization.

 Superconductivity: It is a property of certain materials where electrical resistance drops to zero and magnetic fields are expelled from the interior (Meissner effect) below a critical temperature (T_c). According to BCS theory, superconductivity arises due to the formation and condensation of Cooper pairs. When an electron moves through the lattice, it slightly distorts the positively charged ions, creating a region of increased positive charge. This distortion can attract another electron with opposite momentum and spin, leading to an effective attractive interaction and the formation of a Cooper pair.

• Josephson effect: The passing of super-current between two superconductors separated by a weak link is called is Josephson effect. This happens due to the quantum tunneling of Cooper pairs. The amount of current is governed by the equation:

$$I = I_c \sin \phi \tag{2.3}$$

Where:

- I_c is the maximum super-current that can pass without applying voltage (critical current),
- ϕ is the phase difference of the superconducting wave functions across the junction.

The critical current through a Josephson junction depends on the size of the junction, the superconducting material, and the operating temperature.

• Magnetic flux quantization: The total magnetic flux enclosed by a closed superconducting loop is quantized, i.e., it can only take values that are integer multiples of the flux quantum Φ_0 (2.07×10⁻¹⁵ Wb). This quantization arises because the macroscopic wave function describing the Cooper pairs must be single-valued around the loop.

There are two types of SQUID: direct current (DC) and radio frequency (RF) SQUID. RF SQUID uses only one Josephson junction, is driven by RF current, and has a low production cost. But they are less sensitive. We will discuss the working of DC SQUID, but not of RF SQUID.

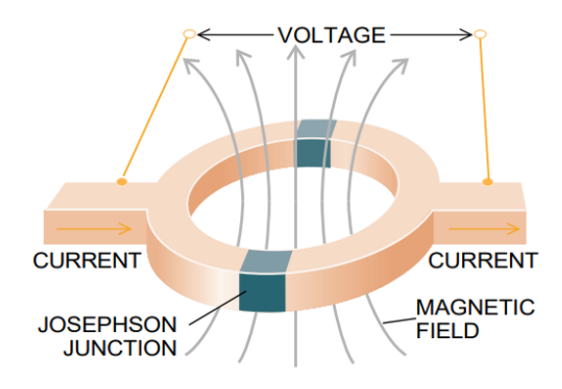


Figure 2.5: Schematics of a basic SQUID Magnetometer[5]

DC SQUID (Figure 2.5) contains two parallel Josephson junctions. When an external magnetic flux Φ is applied, the phase difference across the junctions leads to constructive or destructive interference of the super-currents. As a result, the total critical current I_c of the SQUID oscillates periodically with Φ . If a bias current greater than this I_c is applied, a voltage develops across the SQUID that also varies periodically with Φ . Thus, small changes in magnetic flux can be detected by measuring the corresponding changes in voltage.

VSM

The vibrating sample magnetometer works on the basis of Faraday's law of induction. The sample is placed in a constant external magnetic field, which aligns the

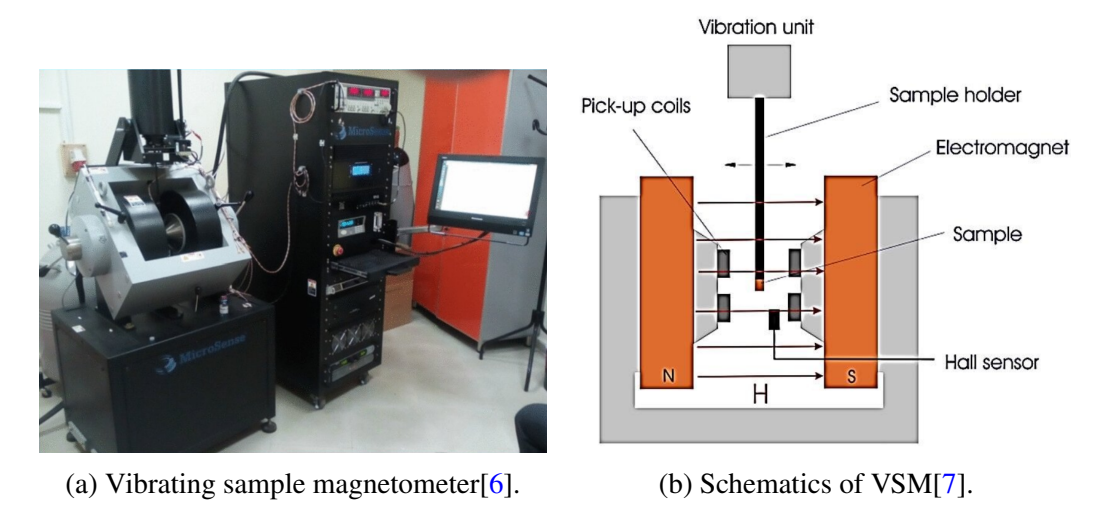


Figure 2.6

magnetic moments of the magnetic sample in its direction according to the strength of the applied field. The sample is then vibrated, which changes the magnetic field (created by the magnetic dipole moments of the sample) with time, thus creating an electric field in the pickup coil. This electric field can give information about the magnetization properties of the sample. A graph of magnetization versus magnetic field strength can be obtained by varying the strength of the external magnetic field.

Chapter 3

Results and Discussion

3.1 Fe₃GeTe₂

3.1.1 Initial CVT Sample

Following the CVT synthesis described in Section 2.1.1, PXRD was performed. The sample, initially in pellet form, was ground into a powder for measurement. PXRD was used to verify the formation of the Fe₃GeTe₂ crystalline phase.

By comparing the measured data (3.1a) with reference data (3.1b), we find that the sample was not formed in the required phase.

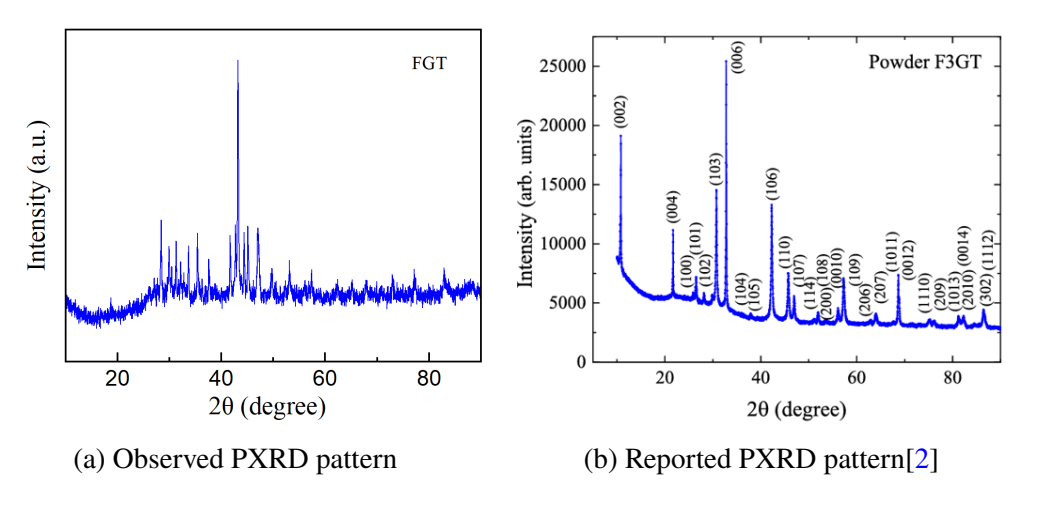


Figure 3.1

3.1.2 Polycrystalline Sample

Switching to solid-state synthesis, the resulting polycrystalline powder was analyzed via PXRD. The recorded profile (Figure 3.2) matched with the ones reported

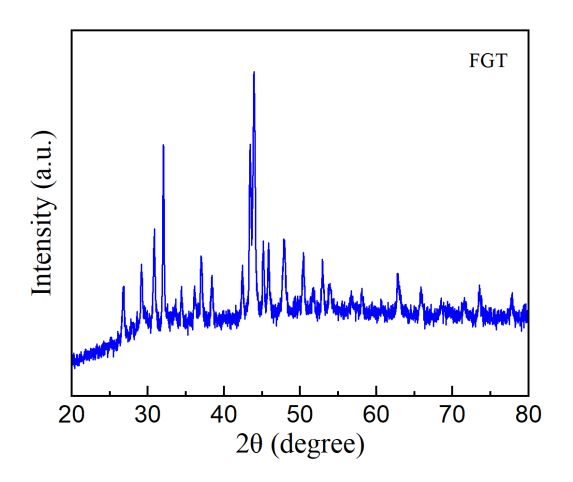


Figure 3.2: Observed PXRD pattern

in the literature (Figure 3.3), though the overall intensity was low, and the peaks

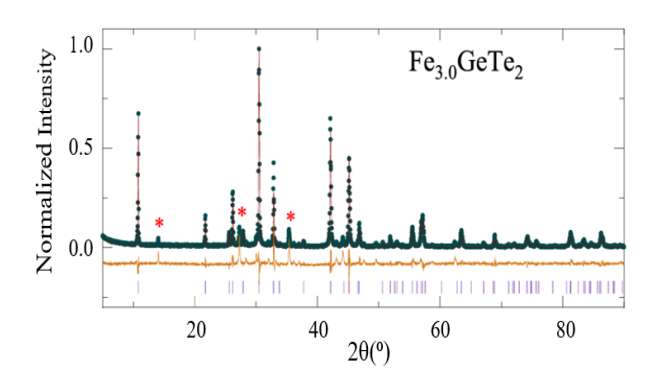


Figure 3.3: Reported PXRD [8].

were broad and slightly shifted.

3.1.3 Single Crystal Sample

Single crystals in the form of rods were obtained as a result of the synthesis process described in Section 2.1.2. The single Crystals thus obtained and the powder residue were collected for PXRD. While comparing the measured data

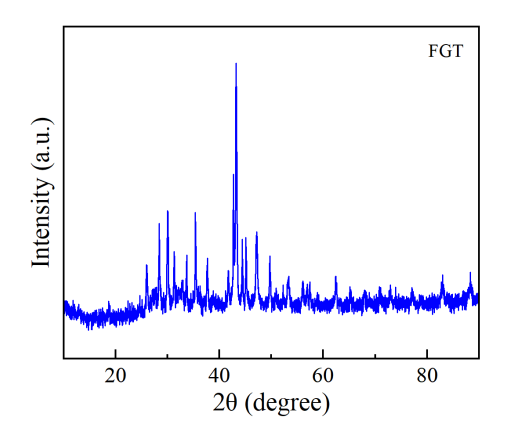


Figure 3.4: Observed PXRD pattern

(Figure 3.4) with reference data (Figure 3.3), it was found that the sample was not formed again.

EDX Analysis

| Element | Weight % | Atomic % |
|---------|----------|----------|
| Fe K | 73.2 | 78.1 |
| Ge K | 26.6 | 21.9 |
| Te L | 0.2 | 0.1 |

Table 3.1: EDX data.

An EDX analysis was carried out to determine the cause of the unsuccessful material formation. The EDX results (Table 3.1) showed that the atomic percentage of Tellurium is only 0.1%. This indicates that the tellurium gets evaporated from the sample during preparation.

3.1.4 Te Compensation and Characterization

After the tellurium compensation process described in Section 2.1.3, PXRD and resistance measurements were performed on the sample.

The resulting PXRD data (Figure 3.5a) indicated that there was significant noise, suggesting the presence of impurities. The plot (Figure 3.5b) confirmed metallic behavior, consistent with previous reports [9]. However, Raman spectroscopy did not detect any peaks.

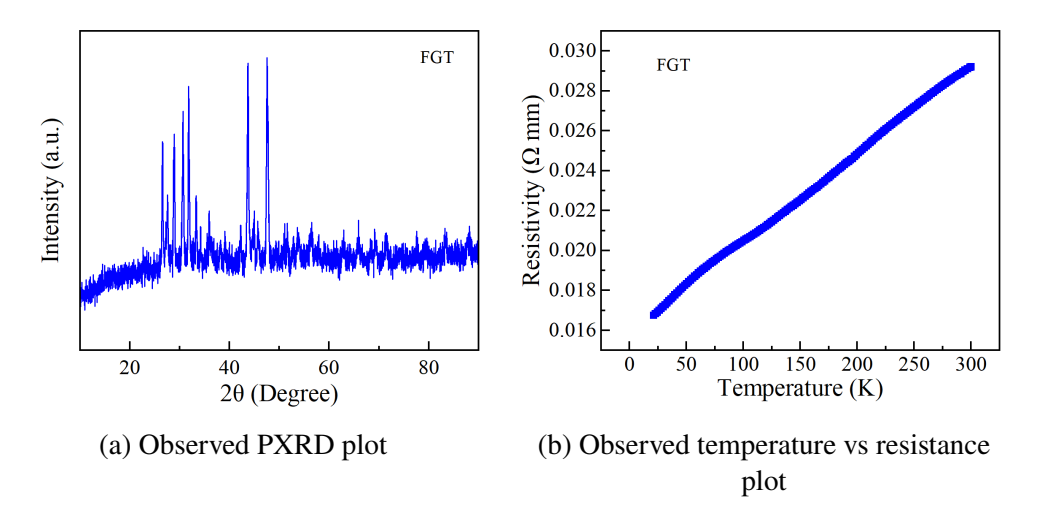


Figure 3.5

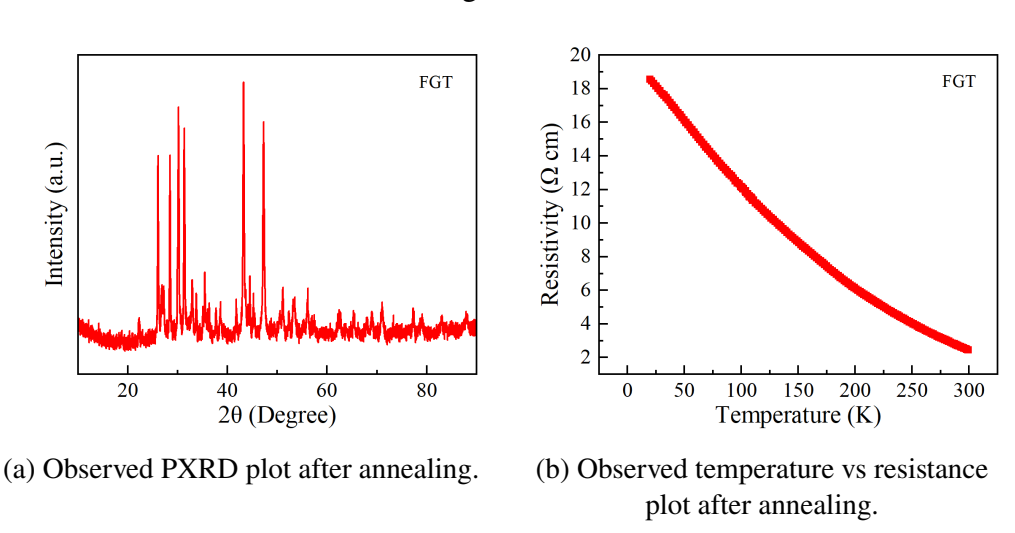


Figure 3.6

Following the annealing process mentioned in Section 2.1.3, done in order to improve crystallinity and to get the desired phase, the same characterization techniques were repeated. This time, not only did Raman spectroscopy again fail to show any peaks, but the temperature vs. resistance plot (Figure 3.6b) also indicated semiconducting behavior instead of metallic. The PXRD measurements (Figure

3.6a) remained similar to those obtained earlier, even though the crystallinity improved.

These findings led to the conclusion that the intended material could not be successfully synthesized. As repeated efforts also proved unsuccessful, the focus was shifted toward synthesizing a different 2D magnetic material.

$3.2 VSe_2$

3.2.1 Solid-State Synthesized VSe₂

Following the synthesis process described in Section 2.2.1, where complete melting of vanadium was achieved, EDX analysis was conducted to determine the stoichiometry of the synthesized sample. The EDX results indicated an excess of selenium.

| Element | Atomic % | Error % |
|---------|----------|---------|
| V | 23.6 | 4.4 |
| Se | 76.4 | 5.3 |

After the annealing process mentioned in Section 2.2.1, several characterizations were done in order to find whether the proper stoichiometric samples were formed.

The PXRD data (Figure 3.7a) aligns with the reference pattern (Figure 3.7b), although there are differences in peak intensities. Similarly, the Raman spectra

(Figure 3.8a) match the reported data (Figure 3.8b), confirming structural consistency.

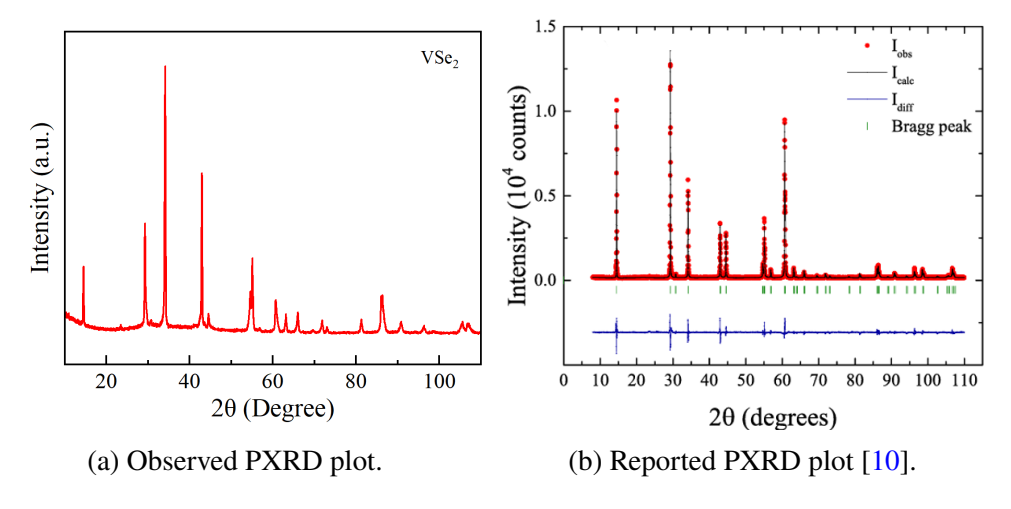


Figure 3.7

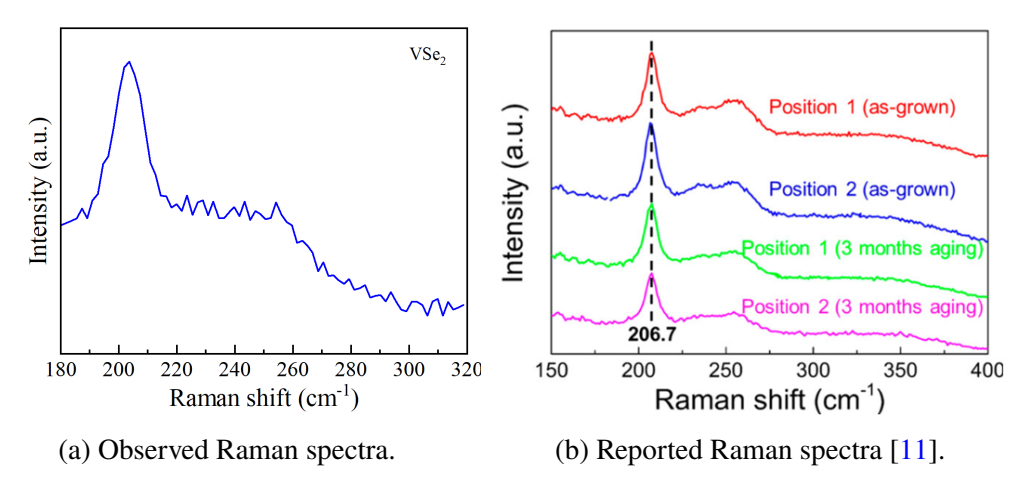
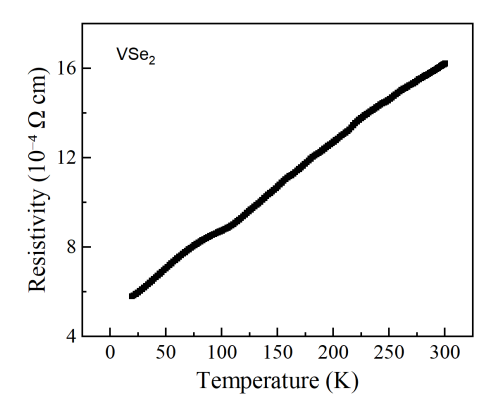
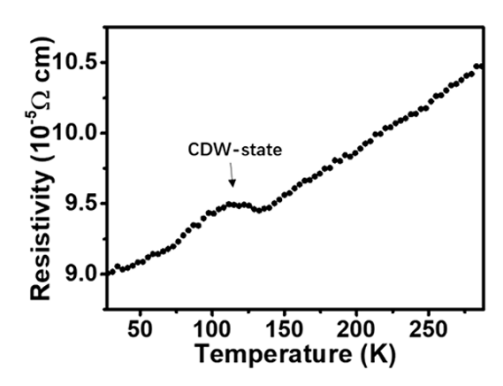


Figure 3.8

The temperature dependence of the resistivity plot (Figure 3.9a) reveals a charge density wave (CDW) transition around 100°C, though it is less pronounced than previously reported (Figure 3.9b).





- (a) Observed temperature dependence of the resistivity.
- (b) Reported temperature dependence of the resistivity [12].

Figure 3.9

EDX measurement was conducted to determine the stoichiometry of the sample. The EDX data (Table 3.2) indicates an excess of selenium in the sample.

| Element | Atomic % | Error % |
|---------|----------|---------|
| V | 29.4 | 3.8 |
| Se | 70.6 | 7.4 |

Table 3.2: EDX data.

Since both the PXRD data and Raman spectra correspond to the reference, it can be concluded that VSe₂ has formed in desired phase. However, the presence of excess selenium, as indicated by the EDX analysis, suggests that the sample contains defects.

3.2.2 CVT Synthesized VSe₂

After the synthesis process mentioned in Section 2.2.2, single crystals in the form of flakes (Figure 3.10) were obtained at the center of the quartz tube, while polycrystals formed at the hot end.

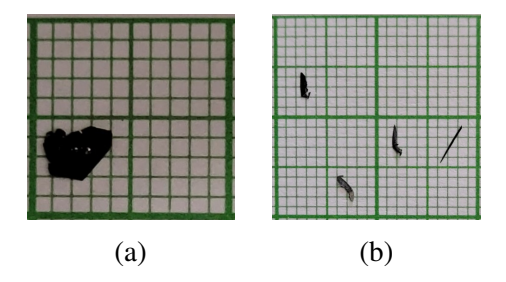
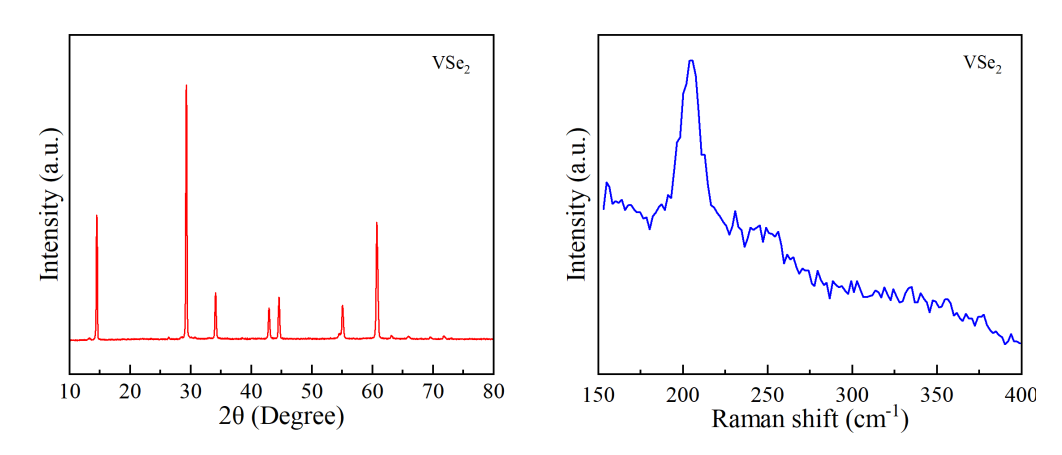


Figure 3.10: Single crystals

Various characterization techniques were employed to determine whether the desired material had been successfully synthesized.



(a) Observed PXRD plot of polycrystals. (b) Observed Raman spectra of polycrystals.

Figure 3.11

The PXRD data (Figure 3.11a) and Raman spectra (Figure 3.11b) of the poly-

crystals closely matched previously reported results, although differences in PXRD peak intensities were observed.

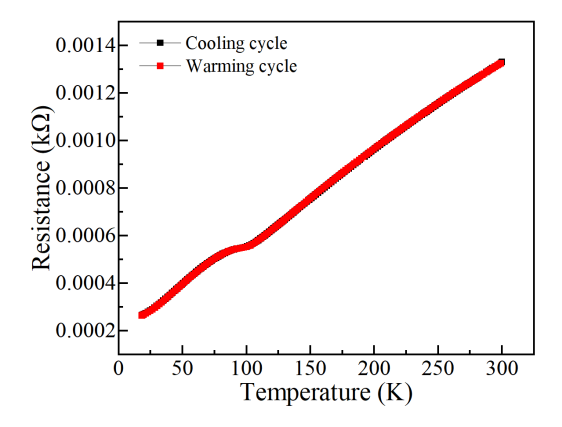


Figure 3.12: Temperature vs resistance plot of single crystal

The temperature vs. resistance plot of the single crystal (Figure 3.12) displayed a charge density wave (CDW) transition at approximately 90 K, slightly lower than the previously reported 100 K.

| Element | Atomic % | Error % |
|---------|----------|---------|
| V | 26.0 | 4.0 |
| Se | 74.0 | 4.9 |

Table 3.3: EDX data of single crystal.

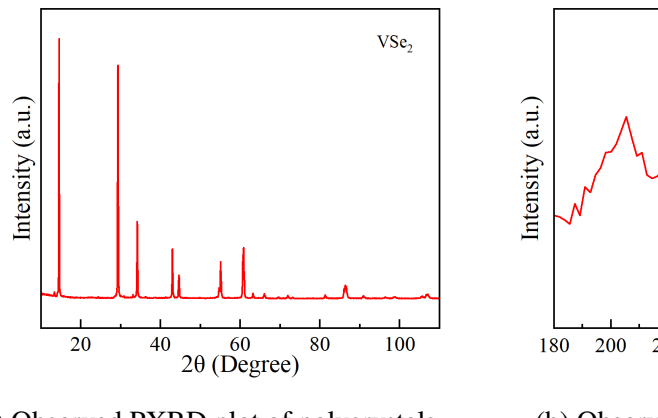
EDX analysis (Table 3.3) revealed that the single crystals contained an excess of selenium, whereas the poly-crystals (Table 3.4) exhibited a selenium deficiency.

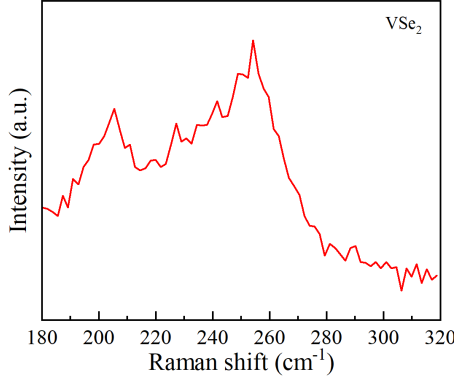
Based on these characterizations, it was concluded that the desired structure had formed. However, there is an excess of selenium in the single crystals and a deficiency in the polycrystals.

| Element | Atomic % | Error % |
|---------|----------|---------|
| V | 35.3 | 3.7 |
| Se | 64.7 | 5.3 |

Table 3.4: EDX data of polycrystal VSe₂.

Characterization was performed after the annealing process—carried out to obtain a properly stoichiometric sample as described in Section 2.2.3—to evaluate whether the resulting polycrystalline material had the correct stoichiometry.





- (a) Observed PXRD plot of polycrystals after annealing.
- (b) Observed Raman spectra of polycrystals after annealing.

Figure 3.13

The PXRD pattern (Figure 3.13a) closely resembles the reported data, although differences in peak intensities were observed. Raman spectroscopy (Figure 3.13b) revealed an additional peak.

The temperature vs. resistivity plot (Figure 3.14) confirmed the metallic nature of the sample. However, other than the expected charge density wave (CDW) transition, there was an additional transition.

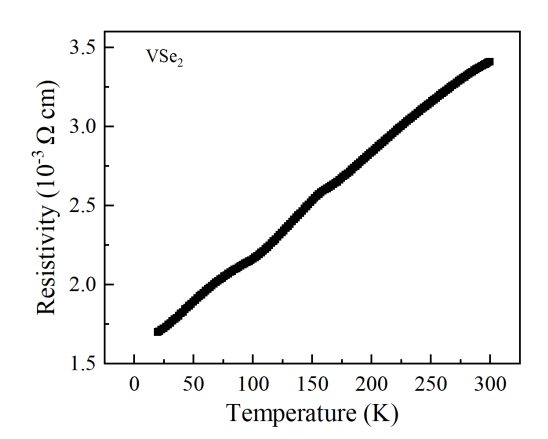


Figure 3.14: Temperature vs resistivity plot of Polycrystals after annealing

Based on these findings, it can be concluded that a proper stoichiometric sample was not obtained. Due to the time constraints, it was decided to leave the synthesis of 2D magnetic materials.

3.3 Magnetic measurements

Magnetic characterization, including magnetization versus temperature and magnetization versus applied field measurements, was performed on 2D materials such as ZrSe₂, Zirconium-rich ZrSe₂, ZrSe₃, TiSe₂, and Zr-doped TiSe₂, which were synthesized by fellow lab mates.

3.3.1 ZrSe₂

Zirconium has the electronic configuration [Kr] $4d^2 5s^2$, while selenium has [Ar] $3d^{10} 4s^2 4p^4$. When these elements combine to form ZrSe₂, all electrons

are expected to be paired, indicating no unpaired electrons. Therefore, ZrSe₂ is anticipated to exhibit diamagnetic behavior. This expectation was confirmed through magnetic measurements (Figure 3.15), which verified that ZrSe₂ is indeed diamagnetic.

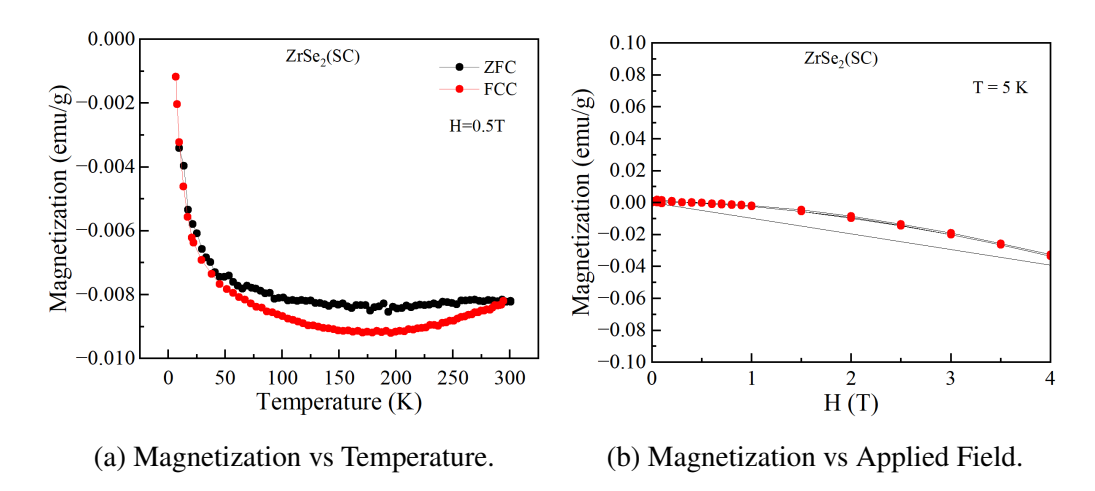


Figure 3.15

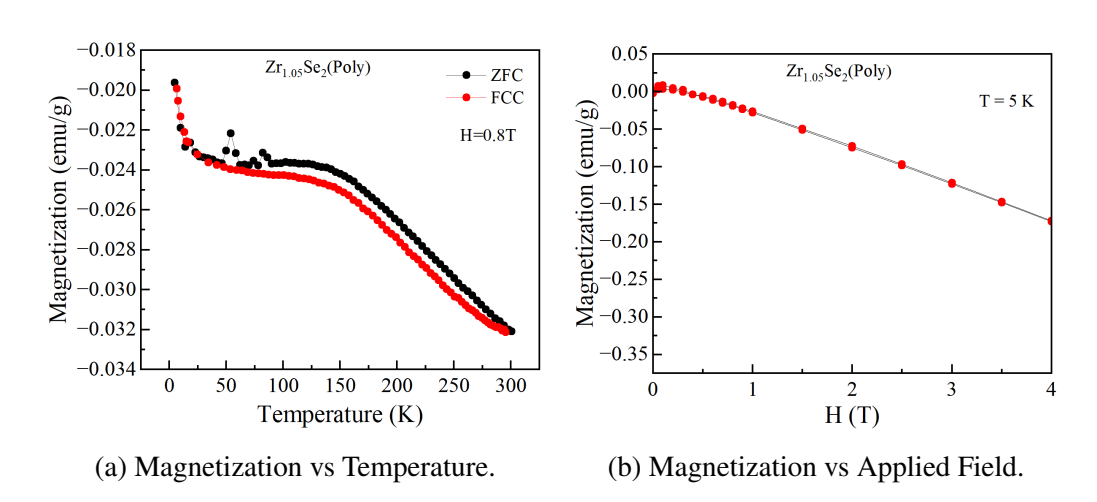


Figure 3.16

Magnetic measurements on ZrSe2 with a slight excess of zirconium revealed an

enhancement in its diamagnetic behavior compared to the stoichiometric ZrSe₂. As expected for a diamagnetic material, an opposing magnetic field is induced within the sample (Figure 3.16b). Although the magnetization remains negative, a bifurcation is observed between the zero-field-cooled (ZFC) and field-cooled cooling (FCC) curves (Figure 3.16a). This divergence may be attributed to exchange interactions arising from unpaired electrons associated with the excess zirconium.

3.3.2 **ZrSe**₃

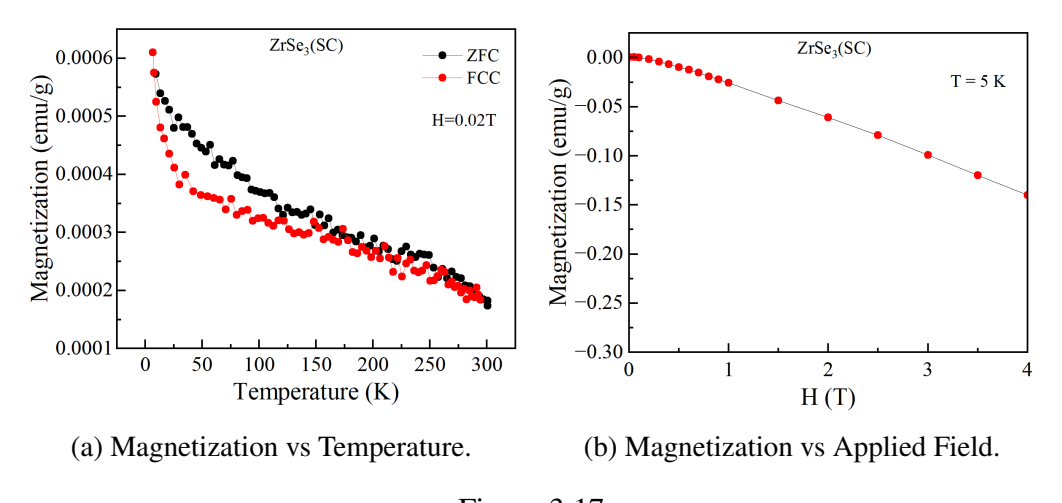


Figure 3.17

The magnetization versus temperature measurement (Figure 3.17a) indicates paramagnetic behavior at lower magnetic fields, as evidenced by the inverse relationship between magnetization and temperature consistent with Curie's law. However, under higher applied magnetic fields, the material exhibits diamagnetic behavior as shown in Figure 3.17a.

3.3.3 TiSe₂

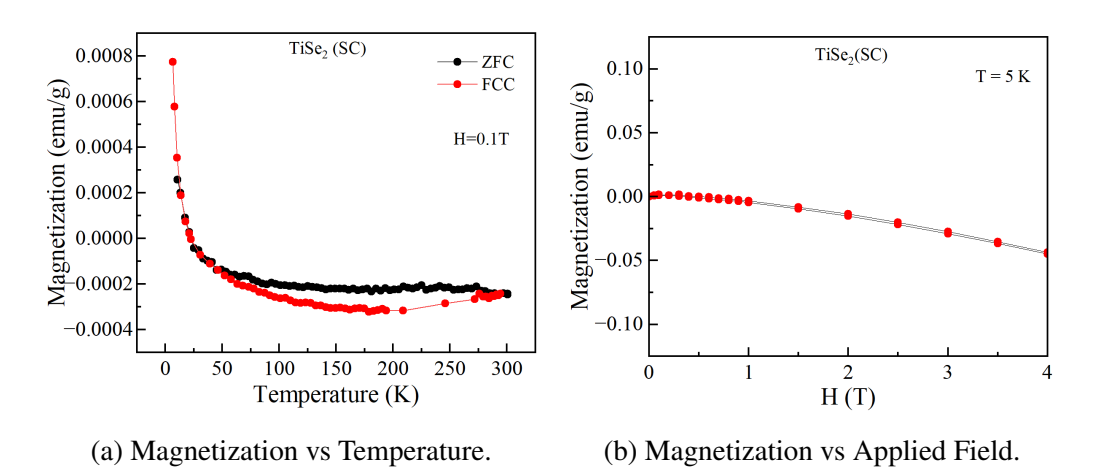


Figure 3.18

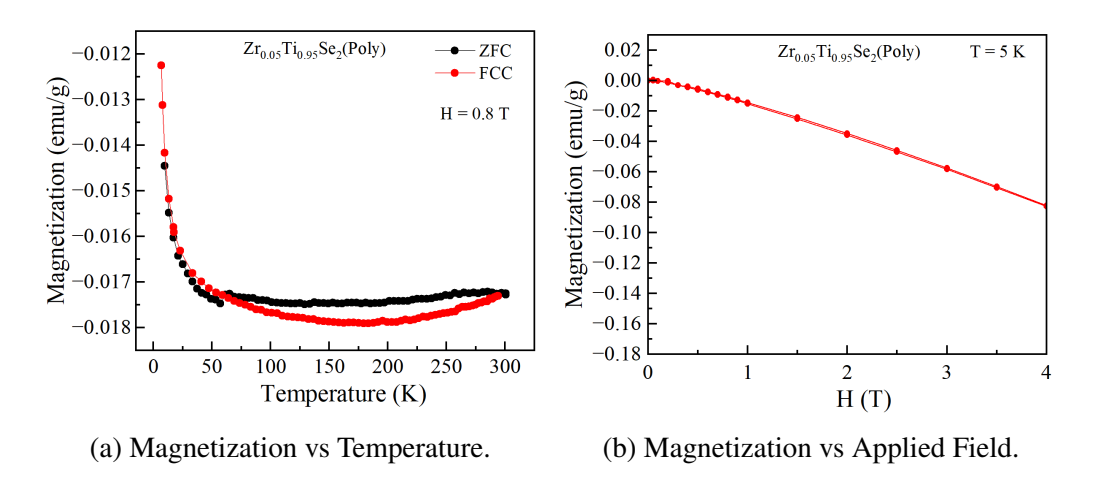


Figure 3.19

In TiSe₂, all electrons are paired, so the magnetization versus temperature measurement is expected to show a temperature-independent negative value, characteristic of diamagnetic behavior. However, Figure 3.18a displays a slight paramagnetic upturn at lower temperatures. In the magnetization versus applied field

measurement (Figure 3.18b), this slight paramagnetic behavior is observed at very low fields. This deviation may result from the presence of unpaired electrons caused by a slight off-stoichiometry in the TiSe₂ composition.

Upon doping $TiSe_2$ with 5% zirconium, the slight paramagnetic upturn observed at lower temperatures in pure $TiSe_2$ is no longer present (Figure 3.19), and the material exhibits an enhanced diamagnetic character.

Chapter 4

Conclusion

In this study, we explored the synthesis and magnetic properties of two-dimensional (2D) magnetic materials, with a primary focus on Fe₃GeTe₂ and VSe₂. Despite multiple synthesis attempts using chemical vapor transport (CVT) and solid-state methods, phase-pure Fe₃GeTe₂ could not be successfully obtained, primarily due to tellurium loss during the process. On the other hand, phase-pure VSe₂ was successfully synthesized, although achieving the correct stoichiometry remained a challenge.

We also investigated the magnetic behavior of other 2D materials such as ZrSe₂, ZrSe₃, TiSe₂, and Zr-doped TiSe₂, synthesized by fellow lab members. Magnetic measurements confirmed diamagnetic behavior in ZrSe₂ and TiSe₂, with slight paramagnetic features observed in off-stoichiometric or doped samples. Notably, ZrSe₃ exhibited a transition from paramagnetic to diamagnetic behavior under increasing magnetic field. Furthermore, doping TiSe₂ with zirconium was

found to suppress its low-temperature paramagnetic upturn, thereby enhancing its diamagnetic nature.

These findings highlight the critical influence of stoichiometry, structural defects, and elemental doping in tailoring the magnetic properties of 2D materials. Such tunability is essential for the practical application of 2D magnets in spintronic devices, where precise control over magnetic ordering and thermal stability is required. This work also demonstrates that inducing magnetism in intrinsically non-magnetic 2D materials remains a significant challenge.

Future efforts can be directed toward improving phase purity and stoichiometric control during synthesis, as well as investigating these materials at the monolayer limit to further understand their magnetic behavior and potential for integration into nanoscale magnetic and spintronic technologies.

Bibliography

- [1] Mathias G. *Fundamentals of Magnetism*. Springer-Verlag Berlin Heidelberg, Berlin, Heidelberg, first edition, 2008.
- [2] Rosni R. and Rajib M. Anisotropic magnetic, magnetocaloric properties, and critical behavior studies of cvt-grown single-crystalline fe_{3-x}gete₂. *Phys. Rev. B*, 109:024416, 2024.
- [3] Dian Li, Xiong Wang, Chi ming Kan, Daliang He, Zejun Li, Qing Hao, Hongbo Zhao, Changzheng Wu, Chuanhong Jin, and Xiaodong Cui. Structural phase transition of multilayer vse₂. *ACS Appl.Mater. Interfaces*, 12:25143–25149, 2020.
- [4] Andrew F. May, Stuart C., Claudia C., Huibo C., and Michael A.M. Magnetic structure and phase stability of the van der waals bonded ferromagnet fe_{3-x}gete₂. *Phys. Rev. B*, 93:014411, 2016.
- [5] John C. Squids. *Scientific American*, 271:46–53, 1994.
- [6] M'hamed O., Abderrahmane Y., Omar T., and Rachid I. Assessing the impact of magnetic circuit corrosion on the magnetic performance of induction machines. *Electr. Eng.*, 106(4):4091–4101, 2024.

- [7] Mohsin R. Study of the Magnetoelectric Properties of Multiferroic Thin Films and Composites for Device Applications. PhD thesis, COMSATS Institute of Information Technology, 2015.
- [8] Daniel A.M., George D.A. Wood, Samuel J.R. Holt, Grady B., Emily J.L.D., Martin R.L., and Geetha B. Effects of fe deficiency and co substitution in polycrystalline and single crystals of fe_xgete₂. 2021.
- [9] P. Saha, M. Singh, V. Nagpal, P. Das, and S. Patnaik. Scaling analysis of anomalous hall resistivity and magnetoresistance in the quasi-two-dimensional ferromagnet fe_x gete₂. *Phys. Rev. B*, 107:035115, 2023.
- [10] Sourabh B., M. Ciomaga Hatnean, M. R. Lees, and G. Balakrishnan. Signatures of the kondo effect in vse₂. *Nat. Sci. Rep.*, 7:10964, 2017.
- [11] Asad F., Hong R.N., Yun Chang P., Jin-Hyeon J., Myung-Hwa J., Je-Ho L., Jin-Hyeok K., Maeng-Je S., Suklyun H., Seung-Hyun C., and Sunghun L. In-depth structural characterization of 1t-vse₂ single crystals grown by chemical vapor transport. *Cryst.Growth Des.*, 20:2860–2865, 2020.
- [12] Xiong W., Dian L., Zejun L., Changzheng W., Chi-Ming C., Gang C., and Xiaodong C. Ferromagnetism in 2d vanadium diselenide. ACS Nano, 15:16236–16241, 2021.